International Journal of Minerals, Metallurgy and Materials
Volume 30, Number 1, January 2023, Page 82
https://doi.org/10.1007/s12613-022-2472-x

Designing new low alloyed Mg–RE alloys with high strength and ductility via high-speed extrusion

Jinshu Xie[1)], *Zhi Zhang*[1)], *Shujuan Liu*[2)], *Jinghuai Zhang*[1),✉], *Jun Wang*[3),✉], *Yuying He*[1)], *Liwei Lu*[4),✉], *Yunlei Jiao*[1)], *and Ruizhi Wu*[1)]

1) Key Laboratory of Superlight Material and Surface Technology, Ministry of Education, College of Materials Science and Chemical Engineering, Harbin Engineering University, Harbin 150001, China
2) School of Materials Science and Engineering, Harbin Institute of Technology, Harbin 150001, China
3) Ningbo Branch, Ordnance Science Institute of China, Ningbo 315103, China
4) School of Materials Science and Engineering, Hunan University of Science and Technology, Xiangtan 411201, China
(Received: 18 February 2022; revised: 4 March 2022; accepted: 10 March 2022)

Abstract: Two new low-alloyed Mg–2RE–0.8Mn–0.6Ca–0.5Zn (wt%, RE = Sm or Y) alloys are developed, which can be produced on an industrial scale via relatively high-speed extrusion. These two alloys are not only comparable to commercial AZ31 alloy in extrudability, but also have superior mechanical properties, especially in terms of yield strength (YS). The excellent extrudability is related to less coarse second-phase particles and high initial melting point of the two as-cast alloys. The high strength–ductility mainly comes from the formation of fine grains, nano-spaced submicron/nano precipitates, and weak texture. Moreover, it is worth noting that the YS of the two alloys can maintain above 160 MPa at elevated temperature of 250°C, significantly higher than that of AZ31 alloy (YS: 45 MPa). The Zn/Ca solute segregation at grain boundaries, the improved heat resistance of matrix due to addition of RE, and the high melting points of strengthening particles (Mn, $MgZn_2$, and Mg–Zn–RE/Mg–Zn–RE–Ca) are mainly responsible for the excellent high-temperature strength.

Keywords: magnesium alloys; high-speed extrusion; high strength; high ductility; solute segregation

1. Introduction

Magnesium (Mg) alloys, as the lightest metal structural material with a low density (1.74 g/cm^3) about a quarter that of steel, have significant application potential in aerospace, military hardware, automotive, 3C electronic products, and other fields [1–3]. However, traditional Mg alloys usually have low strength and poor ductility at room temperature and unsatisfactory high-temperature strength, seriously hindering the further wide application of Mg alloys [4].

AZ31 commercial alloy, as the most widely used and mature Mg alloy, has good extrudability and can be used in large-scale industrial production. However, the trade-off between production efficiency and mechanical properties is often unavoidable [5–9]. The high-speed extrusion at a high temperature usually results in relatively low mechanical properties. The yield strength (YS) of most Mg alloys, including AZ31, prepared under high-speed extrusion is usually lower than 200 MPa [10–16]. The strength improvement of AZ31 alloy has always been a research hotspot, but according to current reports, the high-strength AZ31 alloy is generally obtained under low-speed extrusion. For example, Zeng *et al.* [17] prepared AZ31 alloy with high YS (317 MPa) and ductility (14.2%) via low-speed extrusion (about 0.1 m/min). Furthermore, the YS of AZ31 alloy decreases sharply with the increasing temperature [18]. Unsatisfactory mechanical properties are difficult to meet the increasing requirements of industrial applications currently, and therefore, it is of great significance to design the new high-performance Mg alloys that can be produced on a large scale.

Generally, the extrudability of Mg alloys is closely related to the solidus temperature and the melting point of the secondary phases [19]. The high-speed extrusion process would produce considerable friction heat, and once the real temperature exceeds the solidus, initial melting, surface oxidation, and local cracking may occur [12]. In addition, if there are unstable secondary phases, the initial melting may also occur far below the equilibrium solidus temperature. Therefore, in addition to the factors affecting mechanical properties, the above influencing factors for extrudability should be considered in designing new industrial Mg alloys. The addition of rare earth (RE) alloying elements could improve the solidus of Mg alloys and form strengthening phases with high melting point [20]. Mn is generally known to eliminate

✉ Corresponding authors: Jinghuai Zhang E-mail: zhangjinghuai@hrbeu.edu.cn; Jun Wang E-mail: nafion412@163.com; Liwei Lu E-mail: cqullw@163.com

harmful elements, inhibit recrystallization to refine grains, and improve heat resistance for Mg alloys [21]. More recently, Jin *et al.* [22] reported that trace Mn addition to Mg–5Bi–2Al alloy could significantly improve the extrudability of the Mg alloy and simultaneously enhance the strength and ductility. Ca is considered to play a similar role to RE in improving heat resistance and modifying texture, and the co-addition of Ca and Zn has been found to facilitate grain boundary (GB) segregation, thus benefiting the heat resistance of Mg alloys [23–25]. Based on the above analysis, the low-alloyed Mg–RE alloys, namely Mg–2RE–0.8Mn–0.6Ca–0.5Zn (wt%, RE = Sm, Y) are prepared via relatively high-speed extrusion in this work, which is expected to contribute to the development of high-performance Mg alloys for industrial application.

2. Experimental

2.1. Materials preparation

The cast Mg–2Sm–0.8Mn–0.6Ca–0.5Zn (wt%) and Mg–2Y–0.8Mn–0.6Ca–0.5Zn (wt%) alloys were prepared by pure Mg (99.95wt%), pure Zn (99.90wt%), pure Ca (99.95wt%), Mg–10%Mn (wt%), and Mg–25%Sm (wt%) or Mg–25%Y (wt%) master alloys at 750°C under inert atmosphere of CO_2 and SF_6 mixture in electric furnace. After melting and stirring, the melt was cast into a steel mould with diameter of 90 mm at 680°C. The actual chemical compositions were analyzed by an inductively coupled plasma-atomic emission spectrometer (ICP-AES, Thermo iCAP 7400), as listed in Table 1. These as-cast ingots were preheated at 300°C for 2 h to reach the extrusion temperature and then extruded from 80 to 16 mm in diameter with a high die-exit speed of 6 m/min. These two as-extruded alloys were marked as MXZ-Sm and MXZ-Y alloys, respectively. In addition, the standard commercial AZ31 ingot prepared by similar casting processes were purchased and also extruded at the same process for comparison.

2.2. Mechanical properties

The as-extruded alloys were machined to dog-bone-shaped tensile test samples with a gauge length of 20 mm, a width of 4 mm, and a thickness of 2 mm. The tensile samples were tested along the extrusion direction (ED) at a Shimadzu AG-X-plus machine at room temperature (RT) and 250°C, with the initial strain rate of 1×10^{-3} s^{-1}. At least three specimens were tested to ensure the accuracy of data.

Table 1. Chemical compositions of the alloys determined by ICP-AES wt%

Alloy	Mg	Sm	Y	Mn	Ca	Zn
Mg–2Sm–0.8Mn–0.6Ca–0.5Zn	Bal.	2.04 ± 0.11	—	0.72 ± 0.03	0.63 ± 0.02	0.47 ± 0.02
Mg–2Y–0.8Mn–0.6Ca–0.5Zn	Bal.	—	1.91 ± 0.09	0.83 ± 0.02	0.58 ± 0.02	0.51 ± 0.02

2.3. Microstructure characterization

The electron back scattered diffraction (EBSD) analysis was performed by a scanning electron microscope (SEM, FEI Nova400) equipped with Symmetry EBSD detector (Oxford Instruments). All the EBSD data were collected with a scanning step size of 0.3 μm and an acceleration voltage of 20 kV. The samples used to EBSD were polished by a Leica RES101 ion beam milling, and the EBSD data were analyzed by the orientation imaging microscopy software Aztec-crystal 2.1 and HKL Channel 5. Taking 15° as the threshold of high angle grain boundaries (HAGBs, black lines) and low angle grain boundaries (LAGBs, gray lines). A transmission electron microscope (TEM, FEI Talos F200X G2) equipped with energy disperse spectroscope (EDS) was used to characterize the microstructure by bright field (BF), high angle annular dark field (HAADF), and high-resolution TEM (HR-TEM) images and scanning transmission electron microscope (STEM)–EDS mappings at the accelerating voltage of 200 kV. The thin foils for TEM were prepared by mechanical grinding to below 40 μm and followed by ion polishing using a Gatan 591 at −30°C. The data of TEM were dealt with the Digital Micrograph 3.7.

3. Results

Fig. 1 shows the bar surfaces of AZ31 and Mg–2RE–0.8Mn–0.6Ca–0.5Zn (wt%) alloys directly extruded at about 300°C using a die-exit speed of 6 m/min. Under the same high-speed extrusion condition, the surface of the two new Mg–RE alloy bars have a smooth surface without crack, just like AZ31 bar. The tensile curves of as-extruded alloys tested at RT are shown in Fig. 2(a). The average YS and total elongation (EL) in MXZ-Sm alloy are 216 MPa and 17%, and they are 226 MPa and 24% for MXZ-Y alloy, respect-

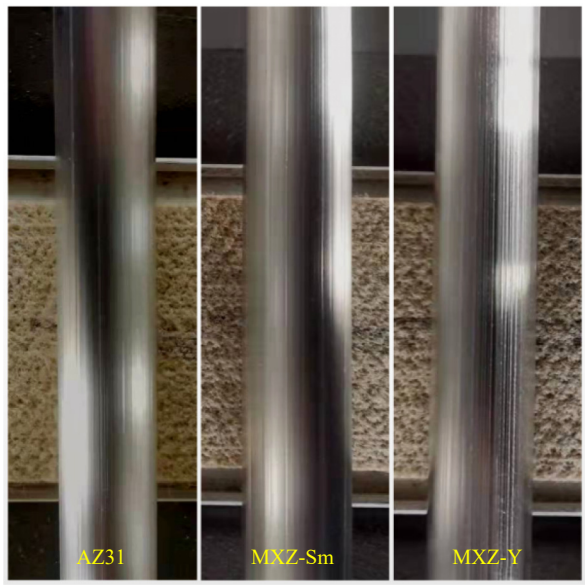

Fig. 1. Extruded bar surfaces of AZ31 and Mg–2RE–0.8Mn–0.6Ca–0.5Zn (wt%) alloys.

ively. Both the two as-extruded alloys show good strength–ductility synergy, and the product of strength and elongation (PSE) for MXZ-Sm and MXZ-Y alloys are 4.131 and 6.408 GPa·%, respectively. It is noted that the AZ31 alloy prepared in the same condition has much lower YS (150 MPa) as compared to the two new alloys. Furthermore, the YS of the two alloys still remains relatively high level tested at high temperature of 250°C, i.e., 165 MPa for MXZ-Sm and 172 MPa for MXZ-Y, only reduced by about 50 MPa compared with the corresponding YS tested at RT (Fig. 2(b)). In contrast, the YS of AZ31 alloy decreases sharply from 150 MPa at RT to 45 MPa at 250°C, which basically fails to meet the application requirements. Table 2 summarizes the YS of high-speed extrusion Mg alloys reported in recent years. Obviously, the newly developed two alloys exhibit the highest YS at RT among these reported alloys, and even the YS values of the two alloys at 250°C are higher than those of most other alloys at RT.

Fig. 3 shows the inverse pole figure (IPF) maps, grain size distribution maps, and (0001) pole figures of as-extruded MXZ-Sm and MXZ-Y alloys. The as-extruded MXZ-Sm alloy consists of almost all dynamic recrystallized (DRXed) fine equiaxed grains, with an average grain size of 2.40 μm by EBSD analysis, while the as-extruded MXZ-Y alloy exhibits higher fraction of un-DRXed grains but lower average grain size (1.76 μm) compared with MXZ-Sm alloy. The orientation of fine DRXed grains are almost random, while the unDRXed grains (blue elongated grains) are certain orientation roughly with <10$\bar{1}$0>//ED. Accordingly, the pole figures show that the MXZ-Y alloy has stronger basal texture than MXZ-Sm alloy. Fig. 4 shows grain orientation spread (GOS) maps and distribution maps of as-extruded MXZ-Sm and MXZ-Y alloys. This is a grain-based method for measuring the local misorientation value of each grain. For each grain, the GOS value was calculated by the average degree of orientation change between every pixel in the grain and the grains average orientation. Here 1° is considered as a threshold to distinguish between DRXed and unDRXed grains, that is, 1° or less for DRXed grains and otherwise larger than 1° for unDRXed grains. Almost all grains are below 1° in MXZ-Sm alloy, while the bimodal distribution in misorientation with one peak at low GOS value and second peak at high GOS value is formed in MXZ-Y alloy. Based on the GOS analysis, the dynamic recrystallization degree of MXZ-Sm alloy is 93.9%, while that of MXZ-Y alloy is 73.6%.

The BF-TEM images further reveal the DRXed grains with grain size of 1.5–3 μm in the as-extruded MXZ-Sm alloy and the DRXed grains with smaller grain size of 1–2 μm in the as-extruded MXZ-Y alloy (Fig. 5). In addtion, micron-scale second-phase particles are rarely found except some

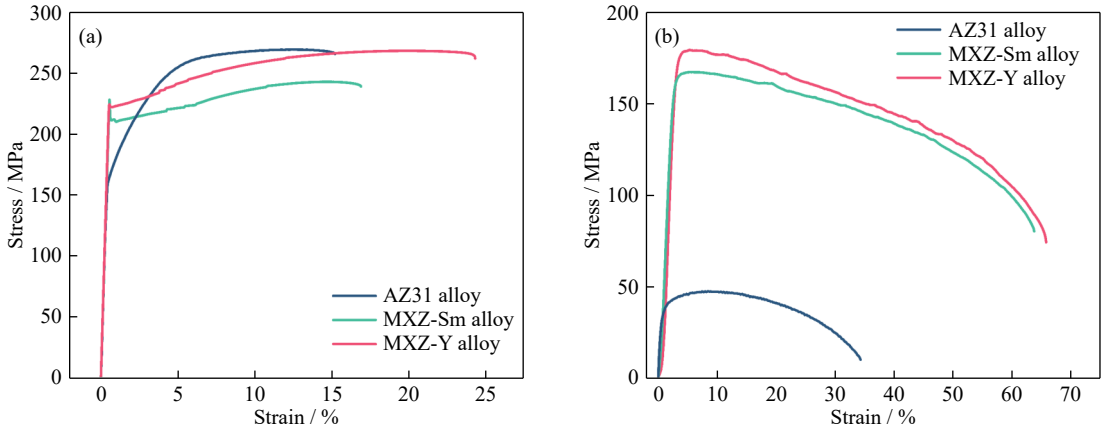

Fig. 2. Tensile stress–strain curves of the as-extruded alloys at (a) 25°C and (b) 250°C.

Table 2. YS of high-speed extruded Mg alloys (extrusion rate: 6 m/min) at room and elevated temperatures

Alloy	Test temperature / °C	YS / MPa	Ref.
Mg–3.36Zn–1.06Sn–0.33Mn–0.27Ca	25	177	[10]
Mg–0.71Zn–0.36Ca–0.07Mn	25	108	[11]
Mg–0.47Mn–0.30Al–0.21Ca	25	207	[12]
Mg–1.58Zn–0.52Gd	25	117	[13]
Mg–5Sn–2Zn	25	132	[14]
Mg–6.81Sn–1.10Al–1.07Zn	25	184	[16]
Mg–5Bi–3Al	25	210	[19]
AZ31	25	150 ± 4	This work
Mg–2Sm–0.8Mn–0.6Ca–0.5Zn	25	216 ± 3	This work
Mg–2Y–0.8Mn–0.6Ca–0.5Zn	25	226 ± 4	This work
AZ31	250	45 ± 4	This work
Mg–2Sm–0.8Mn–0.6Ca–0.5Zn	250	165 ± 2	This work
Mg–2Y–0.8Mn–0.6Ca–0.5Zn	250	172 ± 3	This work

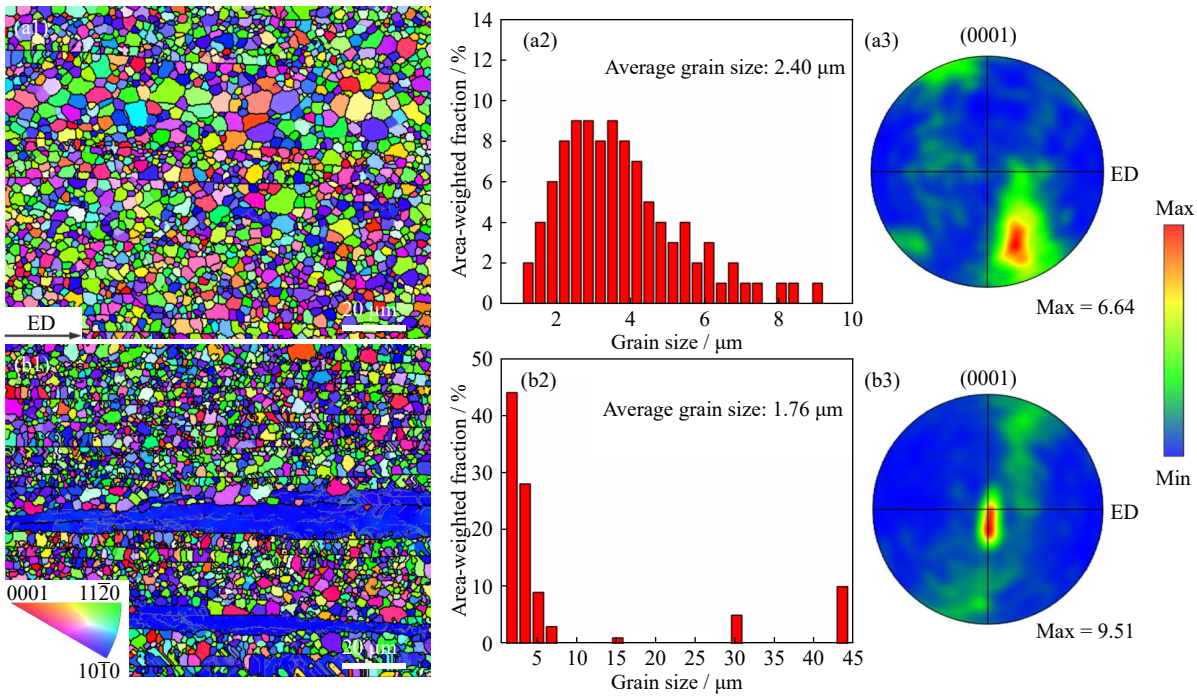

Fig. 3. IPF maps, grain size distribution maps, (0001) pole figures of as-extruded (a1, a2, a3) MXZ-Sm and (b1, b2, b3) MXZ-Y alloys. The reference direction is parallel to ED.

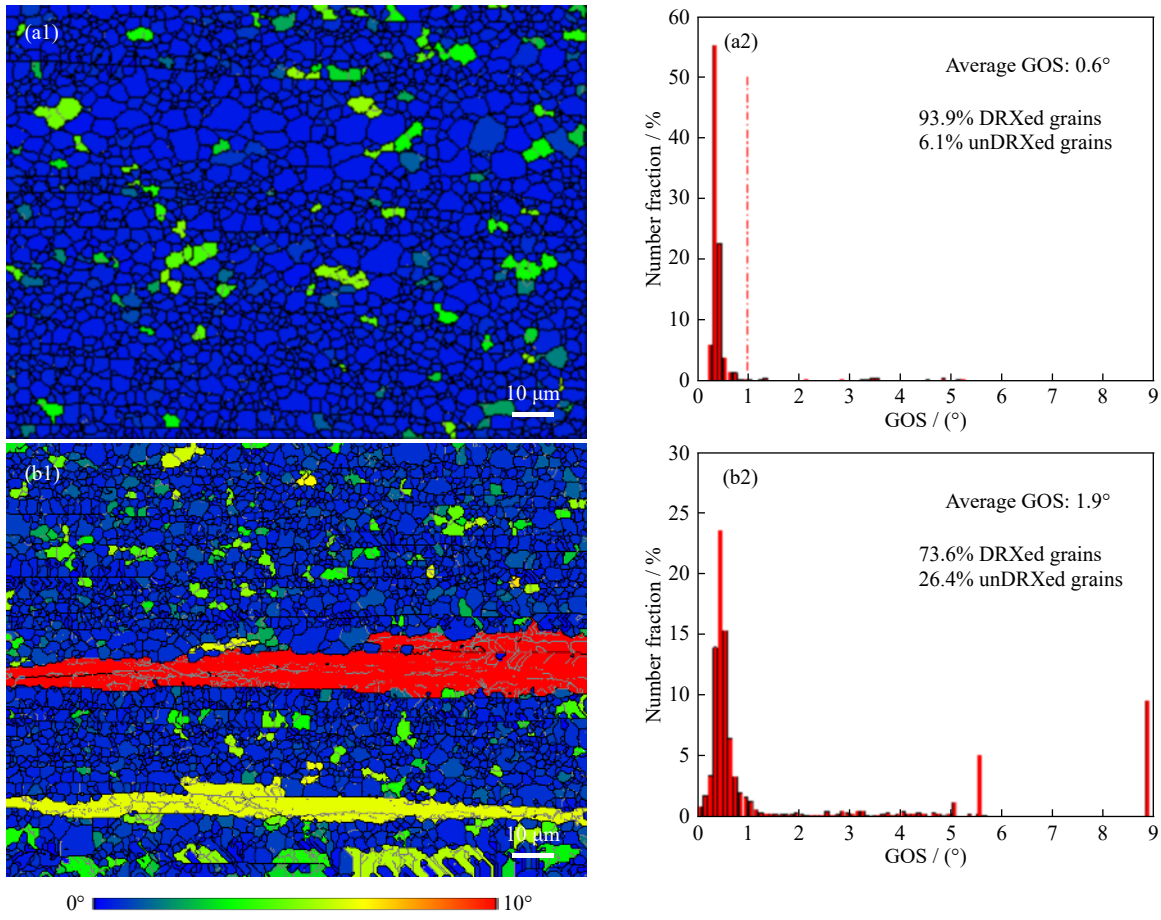

Fig. 4. GOS maps and distribution maps of as-extruded (a1, a2) MXZ-Sm and (b1, b2) MXZ-Y alloys.

submicron particles (green arrows in Fig. 5) in BF-TEM images at low magnification. HAADF-STEM images and corresponding EDS mappings were used to further characterize the second-phase particles in as-extruded alloys. In MXZ-Sm alloy, the particles with size of about 100 nm and above mainly consist of MgZnSm and MgZnSmCa phases (Fig. 6). Most notably, there are a large number of uniformly distributed nanoscale particles in the matrix (Fig. 6). These nano-

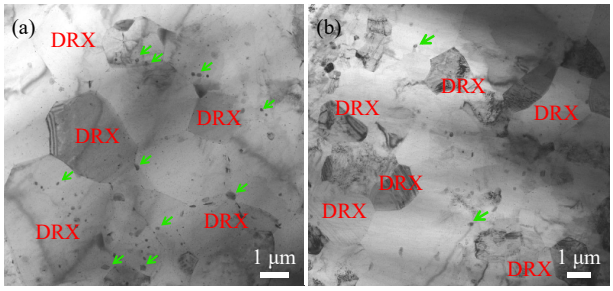

Fig. 5. BF-TEM images of as-extruded (a) MXZ-Sm and (b) MXZ-Y alloys. Submicron particles are marked by the green arrows.

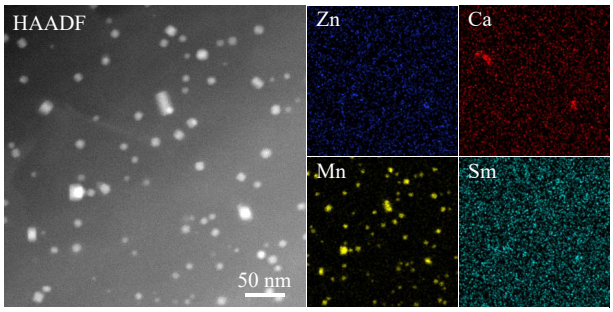

Fig. 6. HADDF-STEM image and corresponding EDS mappings mainly showing particles in as-extruded MXZ-Sm alloy.

particles are confirmed as Mn particles by EDS mappings (Fig. 6). The thickness of the thin foils was measured by the convergent-beam electron diffraction (CBED) method [26], and the effective planar interparticle spacing and uniform diameter of nanoparticles measured using Image-Pro software are 48 and 11.5 nm in MXZ-Sm alloy. HAADF-STEM observation indicates there are almost no sub-micron particles and mainly nanoparticles in MXZ-Y alloy, and EDS mappings suggest that these nanoparticles are composed of Mn particles and Mg–Zn particles (Fig. 7). As for MXZ-Y alloy, the number density of nanoparticles is higher than that for MXZ-Sm alloy, and the effective planar interparticle spacing and uniform diameter of nanoparticles measured by Image-Pro software are 26 and 11.7 nm in MXZ-Y alloy. The HAADF images and the corresponding EDS mappings are also used to characterize the element segregation at GBs in the two as-extruded alloys (Fig. 8). Zn and Ca co-segregation is observed at HAGBs in both the two as-extruded Mg–RE alloys, and part of second-phase particles are found to be distributed at GBs.

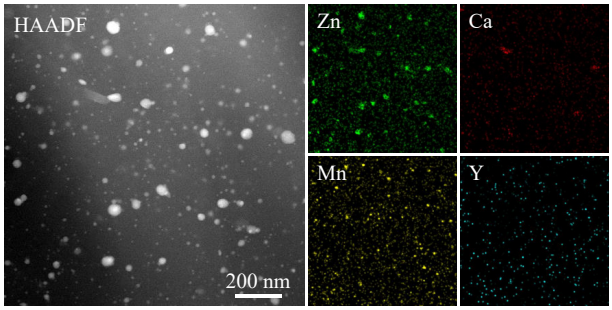

Fig. 7. HAADF-STEM image and corresponding EDS mappings showing nanoparticles in as-extruded MXZ-Y alloy.

Nanoparticles would effectively hinder the movement of dislocations and form a local strain field. It has been reported that Mn nanoparticles are conducive to the accumulation of dislocations on the (0002) plane in Mg alloys [21,27]. Here the geometric phase analysis (GPA) method was used to evaluate the interaction between another nano Mg–Zn phase and dislocations, as shown in Fig. 9. According to the FFT pattern, the Mg–Zn phase has a hexagonal structure and can be identified as $MgZn_2$ phase (the insert image in Fig. 9(a)). Fig. 9(b) and (d) shows the local strain on the (0002) plane is obviously higher than that on the $(01\bar{1}0)$ plane, indicating that the nano $MgZn_2$ particles strongly hinder the most easily activated basal dislocations.

The Kernel average misorientation (KAM) maps and KAM distribution diagrams of two alloys are presented in

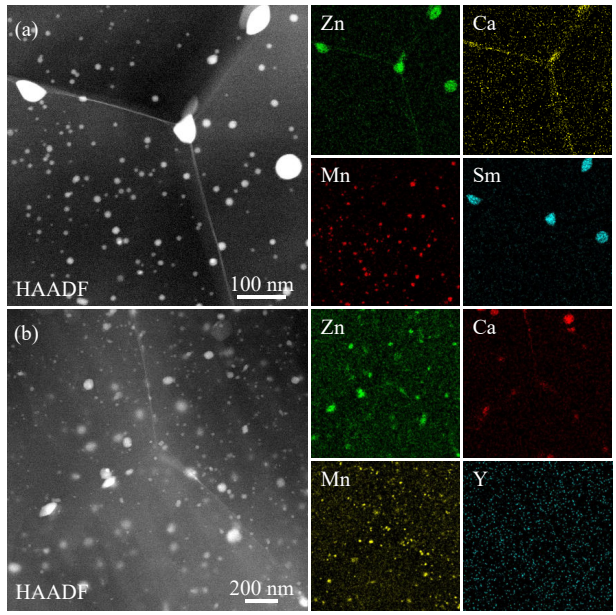

Fig. 8. HAADF-STEM images and corresponding EDS mappings mainly showing GB segregation in as-extruded (a) MXZ-Sm and (b) MXZ-Y alloys.

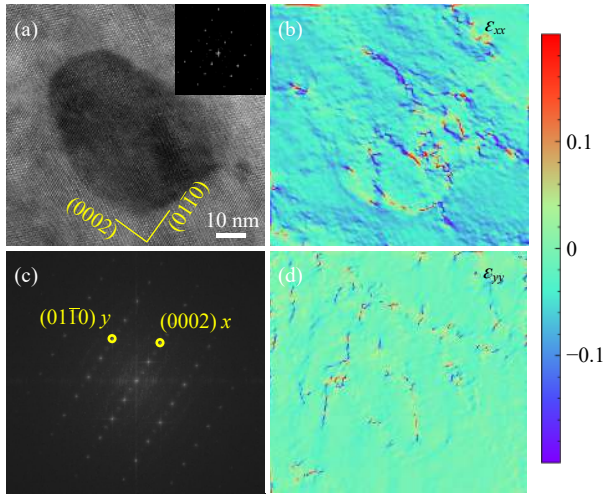

Fig. 9. (a) HR-TEM and Fast Fourier transform (FFT) of $MgZn_2$ phases; (c) FFT pattern of (a); GPA strain distribution of (b) (0002) and (d) $(01\bar{1}0)$ planes. ε_{xx} and ε_{yy} represent axial strain.

Fig. 10. Geometrically necessary dislocations (GND) are accumulated in plastic strain gradient fields and considered necessary to accommodate the local lattice strains. The average KAM value can evaluate the GND density according to the following formula [28–30]:

$$\rho_{GND} = \frac{2\overline{KAM}}{ub} \quad (1)$$

where u can be considered equal to the scanning step of EBSD (300 nm for the two alloys), and b is the magnitude of Burgers vector (about 0.32 nm). The average KAM values of as-extruded MXZ-Sm and MXZ-Y alloys are 0.49° and 0.68°, indicating that the GND densities of the two alloys are 1.78×10^{14} m^{-2} and 2.47×10^{14} m^{-2}, respectively. The difference of dislocations density between the two alloys mainly comes from the relatively lower DRXed fraction of as-extruded MXZ-Y alloy.

Fig. 11 depicts Schmid factor (SF) maps and SF distribution diagrams of as-extruded MXZ-Sm and MXZ-Y alloys. The average SF values of basal slip, prismatic slip, and pyramidal slip in as-extruded MXZ-Sm alloy are 0.32, 0.36, and 0.33, respectively, while they are 0.25, 0.39, and 0.35 in as-extruded MXZ-Y alloy, respectively. Note that there is a more obvious concentration of SF in MXZ-Y alloy, which is related to the bimodal structure containing unDRXed grains in this alloy. Fig. 12 shows the IPFs referring to ED in the two as-extruded alloys. The texture intensity of full grains, DRXed grains, and unDRXed grains are 1.81 multiples of random distribution (mrd), 1.80 mrd, and 3.02 mrd in MXZ-Sm alloy, and they are 8.71 mrd, 1.60 mrd, and 27.38 mrd in MXZ-Y alloy, respectively. Obviously, the stronger texture of MXZ-Y alloy is mainly related to unDRXed grains. Moreover, the DRXed grains with very weak texture intensity of the two alloys have similar two texture components: <11$\bar{2}$1>//ED and <20$\bar{2}$1>//ED. <11$\bar{2}$1>//ED texture is known as a typical "RE texture" [31], that is, the addition of Sm or Y elements obviously weakens the texture of the two as-extruded alloys.

4. Discussion

In this work, two novel low-alloyed MXZ-Sm and MXZ-Y alloys with high strength–ductility at room and elevated temperatures are developed via high-speed extrusion, having great potential for large-scale industrial application. Both alloys exhibit good extrudability comparable to commercial AZ31, and their tensile properties are significantly higher than those of AZ31 as well as most reported high-speed extruded Mg alloys.

4.1. High extrudability of Mg–2RE–0.8Mn–0.6Ca–0.5Zn alloys

It is notable that both the two Mg–2RE–0.8Mn–0.6Ca–0.5Zn alloys without solid solution treatment are success-

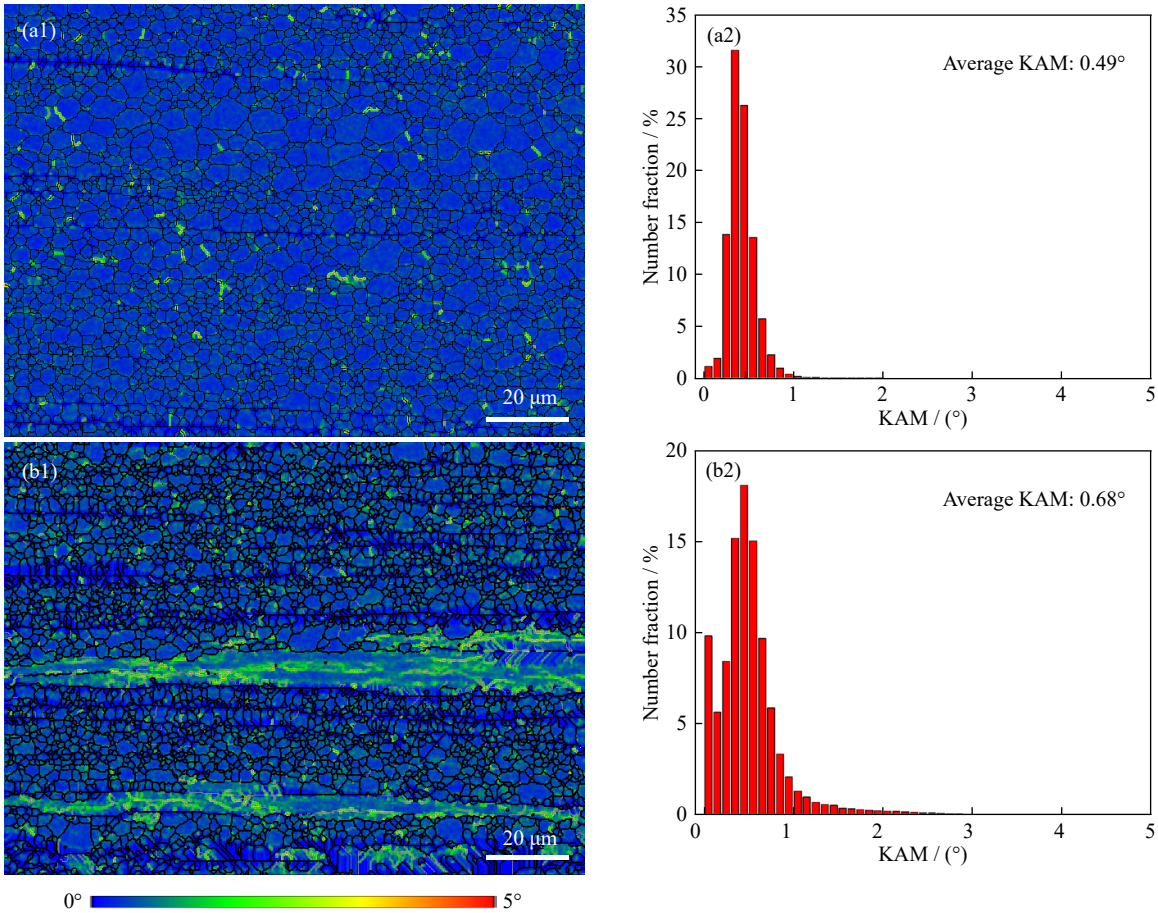

Fig. 10. KAM maps and corresponding KAM distribution histograms of as-extruded (a1, a2) MXZ-Sm and (b1, b2) MXZ-Y alloys.

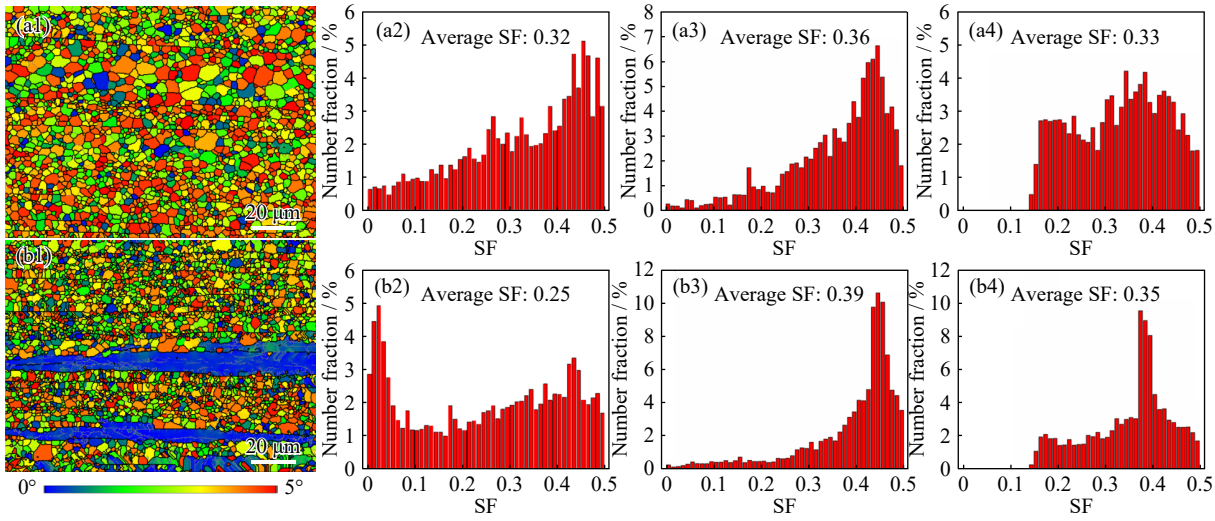

Fig. 11. SF analysis of as-extruded (a1)–(a4) MXZ-Sm and (b1)–(b4) MXZ-Y alloys: (a1, b1) basal slip SF maps; (a2, b2) basal slip SF distribution histogram; (a3, b3) prismatic slip SF distribution histogram; (a4, b4) pyramidal slip SF distribution histogram.

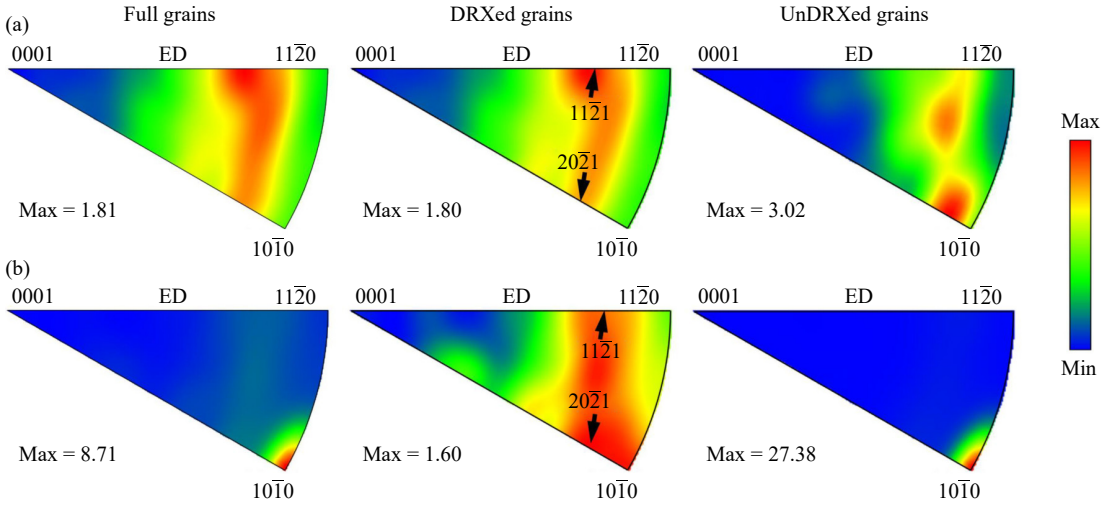

Fig. 12. IPFs with the reference direction parallel to ED of full grains, DRXed grains, and unDRXed grains in as-extruded (a) MXZ-Sm and (b) MXZ-Y alloys.

fully extruded at a high die-exit speed of 6 m/min, showing the crack-free glossy surface just like AZ31 (Fig. 1). Firstly, there are few micron-scale second-phase particles in the as-extruded alloys, and most of them are submicron and nano scale (Fig. 5), suggesting that these second-phase particles mainly come from the dynamic precipitation process during hot-extrusion rather than the block eutectic phase formed during solidification. In other words, there are relatively few secondary phases in these two low-alloyed as-cast alloys, which allows the alloys to be directly extruded without solid solution treatment. Secondly, the extrudability of Mg alloys is related to the thermal stability of the matrix and secondary phases [19]. High-speed extrusion generates considerable heat, and once the local temperature of the die land area is higher than solidus temperature or the melting temperature of secondary phases, local melting and subsequent cracking would occur [12]. For example, severe surface cracks occur in AZ80 and AZ91 alloys extruded at a die-exit speed of 6 m/min or more due to incipient melting of the $Mg_{17}Al_{12}$ phase (melting temperature: 437°C) [16,32]. In contrast, the addition of Sm/Y with high melting point ensures a higher initial melting temperature of the Mg matrix and is conducive to the formation of secondary phases with high melting point (such as Mg–Sm–Zn phase shown in Fig. 6) [20]. Ca element can delay surface oxidation and has a similar effect to RE elements [17,23]. It is believed that the high extrudability of the two new alloys is at least closely related to the above factors.

4.2. High strength and ductility of as-extruded Mg–2RE–0.8Mn–0.6Ca–0.5Zn alloys

The MXZ-Sm and MXZ-Y alloys extruded at a die-exit speed of 6 m/min exhibit YS of 216 and 226 MPa at RT, respectively (Fig. 2(a)), superior to most of the high-speed extruded Mg alloys including AZ31. The high strength of the two alloys is mainly related to the formation of fine grains and a large number of nano particles. As shown in Fig. 3, the average grain sizes for the two alloys are 2.40 and 1.76 μm by EBSD analysis. The formation of fine DRXed grains may be due to the GB segregation and rapid dynamic precipitation of submicron/nano particles hindering the dynamic re-

crystallization process during hot-extrusion [21,23]. It is worth noting that the *k* (Hall-Petch slope) value of Mg alloy is about 290 MPa·μm$^{1/2}$, which is significantly higher than that of Al alloy, indicating that grain refinement could effectively improve the strength of Mg alloy according to Hall-Patch relationship [1,33–34]. STEM observation indicates that the two alloys have abundant dynamic precipitation during hot-extrusion, especially high number density nano-sized precipitates (spacing: 48–26 nm; size: ~12 nm), including Mn, $MgZn_2$, and Mg–RE–Zn particles (Figs. 6–8). Numerous nano-sized precipitates can produce effectively strengthening effect through Orowan mechanism (Fig. 9) [35–36]. In addition to the above two main sources of strengthening, there is still a certain dislocation density (GND densities: 1.78×10^{14} m^{-2} and 2.47×10^{14} m^{-2}) in the two alloys due to the high-speed extrusion at a relatively low temperature of 300°C, also producing strengthening effect to some extent.

More importantly, the two low-alloyed as-extruded Mg–RE alloys can still maintain high strength at elevated temperature, i.e., YS > 160 MPa at 250°C, fundamentally superior to the high-speed extruded AZ31 alloy (YS at 250°C: 45 MPa). Firstly, the high melting point alloying elements such as Sm and Y dissolved into Mg matrix can improve the solidus temperature and heat resistance compared with ordinary Mg alloys such as AZ31 [2,20]. Secondly, different from $Mg_{17}Al_{12}$ with low thermal stability in Mg–Al–Zn alloys, the main precipitation phases in the designed alloys, such as Mn, $MgZn_2$, and Mg–Zn–RE/Mg–Zn–RE–Ca particles, have high melting point, and can still effectively hinder the movement of dislocations at 250°C. Kim *et al.* [37] have reported that the co-existence of $MgZn_2$ and $Ca_2Mg_6Zn_3$ particles in Mg–Zn–Ca alloys improves the thermal stability of the alloy. Thirdly, the Zn/Ca solute element segregation and nanoparticles at GBs also contribute to the heat resistance of the two alloys to maintain high YS at elevated temperature (Fig. 8). Our team [23,25] has found that the Zn/Ca GB segregation can effectively inhibit grain growth at elevated temperature, contributing to a good strengthening effect. Hu *et al.* [38] and Zha *et al.* [39] reported that solute segregation along GBs of nano grains could improve their coarsening resistance by decreasing both GB energy and GB mobility.

The as-extruded MXZ-Sm and MXZ-Y alloys also exhibit excellent ductility at RT, namely EL of 17% in MXZ-Sm alloy and EL of 24% in MXZ-Y alloy, which is related to the following factors. (i) Weak texture. Strong <10$\bar{1}$0>//ED fiber texture, known as the most typical texture in common as-extrued Mg alloys, can be modified by the addition of RE elements. The addition of Sm or Y promotes the formation of a RE texture (i.e., <11$\bar{2}$1>//ED) in DRXed grains and significantly weakens the texture intensity of the two Mg alloys (Fig. 12). EBSD analysis indicates that the basal slip SF is not as low as that of the common extruded Mg alloys with strong basal texture (Fig. 11), meaning that basal dislocation slip is not as difficult as that of the strong-textured common Mg alloys. In addition, high SFs for non-basal dislocation slip system facilitate the activation of non-basal dislocations. Also, it has been reported that RE addition can reduce the critical resolved shear stress (CRSS) ratio of difference between the basal slip and the non-basal slip [40], which is conducive to the activation of non-basal dislocations. For example, Huang *et al.* [40] found adding 5wt% Y can reduce the ratio of $CRSS_{non\text{-}basal}/CRSS_{basal}$ to 1.6–2.7. (ii) Fine grains (2.40 μm for MXZ-Sm and 1.76 μm for MXZ-Y). Fine grains can limit the growth and propagation of twinning, activate the easy-glide <*c*+*a*> dislocation, and suppress the undesirable transition from the easy-glide <*c*+*a*> dislocation to the immobile dislocation [41–43]. For example, Cepeda-Jiménez *et al.* [44] reported that non-basal slip is relatively easy to be activated in pure Mg with grain size of 5 μm than in pure Mg with grain size of 36 μm. In particular, the higher ductility of MXZ-Y alloy may be also related to bimodal structure containing finer DRXed grains. A team [45–46] reported that the coordination between the basal slip in the fine grains at the early stage of deformation and the non-basal slips in the coarse grains at the later stage of deformation helps to accommodate *c*-axis strain, resulting in a high ductility in AZ91–(Sn) alloys.

5. Conclusions

In this work, two highly extrudable low-alloyed Mg–2RE–0.8Mn–0.6Ca–0.5Zn (wt%, RE = Sm or Y) alloys are designed, and the as-extruded alloys show high strength and ductility. The main conclusions are listed as follows.

(1) The MXZ-Sm and MXZ-Y alloys exhibit good extrudability without prior solid solution treatment and still maintain excellent surface quality at a high die-exit speed of 6 m/min. The high extrudability is related to the formation of less coarse eutectic during solidification, and also to the high melting point alloying elements improving the initial melting temperature of the alloy matrix and the secondary phases.

(2) The high-speed extruded MXZ-Sm and MXZ-Y alloys have superior tensile properties (YS > 215 MPa, EL > 15%) at RT than AZ31 alloy extruded at the same process (YS: 150 MPa, EL: 15%). The high strength–ductility of the new alloys is mainly attributed to the formation of fine grains, nano-spaced submicron/nano precipitates, and weak texture.

(3) The high-speed extruded MXZ-Sm and MXZ-Y alloys can still keep high strength at elevated temperature, i.e., YS > 160 MPa at 250°C, fundamentally superior to the high-speed extruded AZ31 alloy (YS: 45 MPa). The excellent high-temperature strength is related to (i) the improved heat resistance of matrix due to the addition of RE, (ii) the formation of strengthening particles (Mn, $MgZn_2$, and Mg–Zn–RE/Mg–Zn–RE–Ca) with high melting points, and (iii) the Zn/Ca GB co-segregation.

Acknowledgements

This work was supported by the National Natural Science Foundation of China (Nos. 52071093 and 51871069), the

Key Laboratory of Micro-Systems and Micro-Structures Manufacturing (HIT), Ministry of Education (No. 2020 KM009), the Student Research and Innovation Fund of the Fundamental Research Funds for the Central Universities (No. 3072022GIP1004), and the Science and Technology Innovation Major Project of Ningbo City, China (No. 2019B10103).

Conflict of Interest

The authors declare that they have no known competing financial interests or personal relationships that could have appeared to influence the work reported in this paper.

References

[1] Z. Zhang, J.H. Zhang, J. Wang, *et al*., Toward the development of Mg alloys with simultaneously improved strength and ductility by refining grain size via the deformation process, *Int. J. Miner. Metall. Mater.*, 28(2021), No. 1, p. 30.

[2] J.H. Zhang, S.J. Liu, R.Z. Wu, L.G. Hou, and M.L. Zhang, Recent developments in high-strength Mg–RE-based alloys: Focusing on Mg–Gd and Mg–Y systems, *J. Magnes. Alloys*, 6(2018), No. 3, p. 277.

[3] M.F. Qi, L.Y. Wei, Y.Z. Xu, *et al*., Effect of trace yttrium on the microstructure, mechanical property and corrosion behavior of homogenized Mg–2Zn–0.1Mn–0.3Ca–*x*Y biological magnesium alloy, *Int. J. Miner. Metall. Mater.*, 29(2022), No. 9, p. 1746.

[4] B.C. Suh, M.S. Shim, K.S. Shin, and N.J. Kim, Current issues in magnesium sheet alloys: Where do we go from here? *Scripta Mater.*, 84-85(2014), p. 1.

[5] J.S. Xie, J.H. Zhang, Z. Zhang, *et al*., New insights on the different corrosion mechanisms of Mg alloys with solute-enriched stacking faults or long period stacking ordered phase, *Corros. Sci.*, 198(2022), art. No. 110163.

[6] L.X. Hong, R.X. Wang, and X.B. Zhang, Effects of Nd on microstructure and mechanical properties of as-cast Mg–12Gd–2Zn–*x*Nd–0.4Zr alloys with stacking faults, *Int. J. Miner. Metall. Mater.*, 29(2022), No. 8, p. 1570.

[7] H. Wu and G.H. Fan, An overview of tailoring strain delocalization for strength–ductility synergy, *Prog. Mater. Sci.*, 113(2020), art. No. 100675.

[8] J. Han, C. Wang, Y.M. Song, Z.Y. Liu, J.P. Sun, and J.Y. Zhao, Simultaneously improving mechanical properties and corrosion resistance of as-cast AZ91 Mg alloy by ultrasonic surface rolling, *Int. J. Miner. Metall. Mater.*, 29(2022), No. 8, p. 1551.

[9] K. Yang, H.C. Pan, S. Du, *et al*., Low-cost and high-strength Mg–Al–Ca–Zn–Mn wrought alloy with balanced ductility, *Int. J. Miner. Metall. Mater.*, 29(2022), No. 7, p. 1396.

[10] M.G. Jiang, C. Xu, T. Nakata, H. Yan, R.S. Chen, and S. Kamado, High-speed extrusion of dilute Mg–Zn–Ca–Mn alloys and its effect on microstructure, texture and mechanical properties, *Mater. Sci. Eng. A*, 678(2016), p. 329.

[11] H.B. Yang, Y.F. Chai, B. Jiang, *et al*., Enhanced mechanical properties of Mg–3Al–1Zn alloy sheets through slope extrusion, *Int. J. Miner. Metall. Mater.*, 29(2022), No. 7, p. 1343.

[12] T. Nakata, T. Mezaki, R. Ajima, *et al*., High-speed extrusion of heat-treatable Mg–Al–Ca–Mn dilute alloy, *Scripta Mater.*, 101(2015), p. 28.

[13] M.G. Jiang, C. Xu, T. Nakata, H. Yan, R.S. Chen, and S. Kamado, Rare earth texture and improved ductility in a Mg–Zn–Gd alloy after high-speed extrusion, *Mater. Sci. Eng. A*, 667(2016), p. 233.

[14] W.L. Cheng, M. Wang, Z.P. Que, *et al*., Microstructure and mechanical properties of high speed indirect-extruded Mg–5Sn–(1,2,4)Zn alloys, *J. Central South Univ.*, 20(2013), No. 10, p. 2643.

[15] F.Z. Meng, S.H. Lv, Q. Yang, *et al*., Multiplex intermetallic phases in a gravity die-cast Mg–6.0Zn–1.5Nd–0.5Zr (wt%) alloy, *J. Magnes. Alloys*, 10(2022), No. 1, p. 209.

[16] S.H. Park, S.H. Kim, H.S. Kim, J. Yoon, and B.S. You, High-speed indirect extrusion of Mg–Sn–Al–Zn alloy and its influence on microstructure and mechanical properties, *J. Alloys Compd.*, 667(2016), p. 170.

[17] Z.R. Zeng, Y.M. Zhu, J.F. Nie, S.W. Xu, C.H.J. Davies, and N. Birbilis, Effects of calcium on strength and microstructural evolution of extruded alloys based on Mg–3Al–1Zn–0.3Mn, *Metall. Mater. Trans. A*, 50(2019), No. 9, p. 4344.

[18] U.M. Chaudry, K. Hamad, and Y.G. Ko, Effect of calcium on the superplastic behavior of AZ31 magnesium alloy, *Mater. Sci. Eng. A*, 815(2021), art. No. 140874.

[19] Y.H. Luo, W.L. Cheng, H. Yu, *et al*., Tailoring the microstructural characteristics and enhancing creep properties of as-cast Mg–5Bi–5Sn alloy through Mn addition, *J. Magnes. Alloys*, 2022. https://doi.org/10.1016/j.jma.2021.12.004

[20] J.S. Xie, J.H. Zhang, Z.H. You, *et al*., Towards developing Mg alloys with simultaneously improved strength and corrosion resistance via RE alloying, *J. Magnes. Alloys*, 9(2021), No. 1, p. 41.

[21] P. Peng, A.T. Tang, J. She, *et al*., Significant improvement in yield stress of Mg–Gd–Mn alloy by forming bimodal grain structure, *Mater. Sci. Eng. A*, 803(2021), art. No. 140569.

[22] S.C. Jin, J.W. Cha, S.H. Joo, and S.H. Park, Enhancing tensile strength and ductility of high-speed-extruded Mg–5Bi–2Al through trace Mn addition, *Mater. Charact.*, 181(2021), art. No. 111500.

[23] Z. Zhang, J.H. Zhang, J.S. Xie, *et al*., Developing a low-alloyed fine-grained Mg alloy with high strength–ductility based on dislocation evolution and grain boundary segregation, *Scripta Mater.*, 209(2022), art. No. 114414.

[24] T.T.T. Trang, J.H. Zhang, J.H. Kim, *et al*., Designing a magnesium alloy with high strength and high formability, *Nat. Commun.*, 9(2018), art. No. 2522.

[25] Z. Zhang, J.H. Zhang, J.S. Xie, *et al*., Significantly enhanced grain boundary Zn and Ca co-segregation of dilute Mg alloy via trace Sm addition, *Mater. Sci. Eng. A*, 831(2022), art. No. 142259.

[26] D.B. Williams and C.B. Carter, *Transmission Electron Microscopy: A Textbook for Materials Science*, 2nd ed., Springer, New York, 2009.

[27] P. Peng, J. She, A.T. Tang, *et al*., A strategy to regulate the microstructure and properties of Mg–2.0Zn–1.5Mn magnesium alloy by tracing the existence of Mn element, *J. Alloys Compd.*, 890(2022), art. No. 161789.

[28] H.C. Pan, G.W. Qin, Y.M. Huang, *et al*., Development of low-alloyed and rare-earth-free magnesium alloys having ultra-high strength, *Acta Mater.*, 149(2018), p. 350.

[29] K. Zhang, Z.T. Shao, C.S. Daniel, *et al*., A comparative study of plastic deformation mechanisms in room-temperature and cryogenically deformed magnesium alloy AZ31, *Mater. Sci. Eng. A*, 807(2021), art. No. 140821.

[30] R. Ni, S.J. Ma, L.J. Long, *et al*., Effects of precipitate on the slip activity and plastic heterogeneity of Mg–11Y–5Gd–2Zn–0.5Zr (wt. %) during room temperature compression, *Mater. Sci. Eng. A*, 804(2021), art. No. 140738.

[31] A. Imandoust, C.D. Barrett, A.L. Oppedal, W.R. Whittington, Y. Paudel, and H.E. Kadiri, Nucleation and preferential growth mechanism of recrystallization texture in high purity binary magnesium–rare earth alloys, *Acta Mater.*, 138(2017), p. 27.

[32] Z. Koren, H. Rosenson, E.M. Gutman, Y.B. Unigovski, and A.

Eliezer, Development of semisolid casting for AZ91 and AM50 magnesium alloys, *J. Light Met.*, 2(2002), No. 2, p. 81.
[33] E.O. Hall, The deformation and ageing of mild steel: III discussion of results, *Proc. Phys. Soc. Sect. B*, 64(1951), No. 9, p. 747.
[34] J. Zhao, B. Jiang, Q.S. Wang, *et al*., Effects of Li addition on microstructures and tensile properties of the extruded Mg–1Zn–*x*Li alloy, *Int. J. Miner. Metall. Mater.*, 29(2022), No. 7, p. 1380.
[35] J.F. Nie, Precipitation and hardening in magnesium alloys, *Metall. Mater. Trans. A*, 43(2012), No. 11, p. 3891.
[36] R. Alizadeh, J.Y. Wang, and J. LLorca, Precipitate strengthening of pyramidal slip in Mg–Zn alloys, *Mater. Sci. Eng. A*, 804(2021), art. No. 140697.
[37] B. Kim, C.H. Hong, J.C. Kim, *et al*., Factors affecting the grain refinement of extruded Mg–6Zn–0.5Zr alloy by Ca addition, *Scripta Mater.*, 187(2020), p. 24.
[38] J. Hu, Y.N. Shi, X. Sauvage, G. Sha, and K. Lu, Grain boundary stability governs hardening and softening in extremely fine nanograined metals, *Science*, 355(2017), No. 6331, p. 1292.
[39] M. Zha, H.M. Zhang, H.L. Jia, *et al*., Prominent role of multiscale microstructural heterogeneities on superplastic deformation of a high solid solution Al–7Mg alloy, *Int. J. Plast.*, 146(2021), art. No. 103108.
[40] Z.H. Huang, L.Y. Wang, B.J. Zhou, T. Fischer, S.B. Yi, and X.Q. Zeng, Observation of non-basal slip in Mg–Y by *in situ* three-dimensional X-ray diffraction, *Scripta Mater.*, 143(2018), p. 44.
[41] Z.X. Wu and W.A. Curtin, The origins of high hardening and low ductility in magnesium, *Nature*, 526(2015), No. 7571, p. 62.
[42] C. Zhang, L. Wu, G.S. Huang, G.G. Wang, B. Jiang, and F.S. Pan, Microstructure and corrosion properties of Mg–0.5Zn–0.2Ca–0.2Ce alloy with different processing conditions, *Rare Met.*, 40(2021), No. 7, p. 1924.
[43] P.F. Qin, Q. Yang, Y.Y. He, *et al*., Microstructure and mechanical properties of high-strength high-pressure die-cast Mg–4Al–3La–1Ca–0.3Mn alloy, *Rare Met.*, 40(2021), No. 10, p. 2956.
[44] C.M. Cepeda-Jiménez, J.M. Molina-Aldareguia, and M.T. Pérez-Prado, Effect of grain size on slip activity in pure magnesium polycrystals, *Acta Mater.*, 84(2015), p. 443.
[45] H. Zhang, H.Y. Wang, J.G. Wang, *et al*., The synergy effect of fine and coarse grains on enhanced ductility of bimodal-structured Mg alloys, *J. Alloys Compd.*, 780(2019), p. 312.
[46] H.Y. Wang, Z.P. Yu, L. Zhang, *et al*., Achieving high strength and high ductility in magnesium alloy using hard-plate rolling (HPR) process, *Sci. Rep.*, 5(2015), No. 1, art. No. 17100.